How to Cite: Saman, D., Bondarenko, L.S., Baimuratova, R.K., Dzeranov, A.A., Dzhardimalieva, G.I., Tropskaya, N.S., & Kydralieva, K.A. (2024) A Statistical Design Approach for an Effective Catalyst in the Fenton Reaction in Case of Fe_3O_4-MOF MIL-88b (Fe) in Methylene Blue Degradation Kinetics. *Eurasian Journal of Chemistry, 29, 3(115), 16–29.* https://doi.org/10.31489/2959-0663/3-24-15

Article

Received: 19 June 2024 | Revised: 2 August 2024 |
Accepted: 12 August 2024 | Published online: 13 September 2024

UDC 544.4+519.242

https://doi.org/10.31489/2959-0663/3-24-15

Daniel Saman[1], Lyubov S. Bondarenko[1,2*], Rose K. Baimuratova[3], Artur A. Dzeranov[1,2,3], Gulzhian I. Dzhardimalieva[1,3], Nataliya S. Tropskaya[1,2], Kamila A. Kydralieva[1]

[1]*Moscow Aviation Institute (National Research University), Moscow, Russia;*
[2]*Sklifosovsky Research Institute for Emergency Medicine, Moscow, Russia;*
[3]*Federal Research Center of Problems of Chemical Physics and Medicinal Chemistry, Russian Academy of Sciences, Chernogolovka, Moscow region, Russia*
*(*Corresponding author's e-mail: l.s.bondarenko92@gmail.com)*

A Statistical Design Approach for an Effective Catalyst in the Fenton Reaction in Case of Fe_3O_4-MOF MIL-88b (Fe) in Methylene Blue Degradation Kinetics

In this paper composites containing metal-organic framework MIL88b(Fe), nanoparticles magnetite (Fe_3O_4) or maghemite (γ-Fe_2O_3) modified by humic acids or ascorbic acid were synthesized and tested in the decomposition reaction of methylene blue. Analysis of predictive model based on multi-factor correlation analysis "physical-chemical properties — concentration of methylene blue after degradation" showed that in a line of selected parameters (initial iron concentration in sample, elemental cell parameter, Fe^{2+}/Fe^{3+} ion ratio on sample surface, total iron ion released concentration, surface area specific, surface charge), a significant factor influencing Fenton reaction kinetics, is only the total concentration of the released iron ions (p-value = 0.0162). The influence of separate Fe^{2+} and Fe^{3+} ions and reaction time on the Fenton reaction kinetics was evaluated by multi-factor analysis. The results demonstrated that concentrations of released iron ions are statistically significant, with a square of the concentration of ions Fe^{2+} and the result of the reaction time to the concentration of ions Fe^{3+}. A comparison of the sign and the coefficient values shows that an increase in ion concentration results in a reduction in methylene blue concentration, thereby accelerating the Fenton reaction rate, with Fe^{2+} ion concentration affecting more than Fe^{3+}. The resulting model is proposed as a means of selecting a sample with the maximum Fenton reaction rate at a given point in time.

Keywords: Fenton reaction, MOFs, methylene blue, degradation kinetics, MIL-88b (Fe), heterogeneous catalysts, predictive model, multivariate correlation analysis.

Introduction

The Fenton reaction is widely used for the oxidation of organic compounds and is characterized by the occurrence of a series of radical chain reactions during the interaction of iron ions and hydrogen peroxide [1, 2]. The most significant contribution to the oxidation process is made by the formation of hydroxyl radicals with the participation of a divalent iron cation according to Equation 1 [3]:

$$Fe^{2+} + H_2O_2 \longrightarrow Fe^{3+} + OH^- + \dot{O}H \quad (1)$$

Despite the absence of restrictions associated with mass transfer, and the relatively high rates of homogeneous Fenton processes, there are a number of disadvantages. These include the need to strictly maintain the pH of the process (pH 2.8–3.5) [4, 5] to achieve optimal catalytic activity, and the formation of a larger amount of ferrous sludge (iron hydroxides/oxides) [6, 7]. To overcome these disadvantages, current research has largely focused on the development of heterogeneous Fenton catalysts [8]. The leaching of metal ions from heterogeneous Fenton reaction catalysts is typically slow, resulting in minimal precipitation during the oxidation process [9]. The reusability and wide pH range performance of most heterogeneous catalysts also make these systems more attractive for advanced oxidation processes with highly active hydroxyl radicals) [10, 11]. Surface ions of divalent and trivalent iron serve as a source of formation of hydroxyl radicals in heterogeneous catalysts for the Fenton reaction [12]. A variety of iron minerals such as hematite, goethite, magnetite, ferrihydrite, pyrite, etc. have already been used in heterogeneous Fenton processes for the degradation of a multitude organic pollutants [13–15]. Porous iron materials are of greatest interest, since the sorption of organic compounds subject to oxidation increases the rate of decomposition [6]. The immobilization of iron compounds using a wide range of traditional porous materials including alumina, carbon black, sili-

con dioxide, zeolite, fibers, biosorbents, hydrogels, etc. is common approach [16–19]. More recently, innovative porous materials known as metal-organic frameworks (MOFs) have been used as heterogeneous Fenton catalysts [20–22].

MOFs are a class of porous materials constructed from metal ions or their clusters connected to each other via organic linkers [23]. The principal advantages of these porous materials are their uniform pore distribution, high surface areas and the possibility of designing the porous structure [24–27]. The pore diameter of these materials can be controlled by varying the nature of the structure-forming element (type of metal and its chelate environment) and the organic bridging linker and its size. Furthermore the possibility of hierarchically combining several coordination polymers into one material, allows for the control, selectivity towards the adsorbate and, in general, functional properties [28–32]. In particular, iron-containing MOF structures, Fe-MOFs, have demonstrated the most significant achievements in the photodegradation of organic pollutants both under visible light and through the Fenton reaction due to the presence of iron-oxo clusters in the structure, as well as high specific surface area values [33]. Such clusters demonstrate their inherent absorption in the visible range and can transfer electrons from O^{2-} to Fe^{3+} [34]. This facilitates the oxidation of organic compounds via the photo-Fenton process [35]. Among all known Fe-MOFs, MIL-88b was previously shown to be the most efficient heterogeneous Fenton catalyst [36], while also exhibiting the highest photocatalytic activity in visible light [37] and biocompatibility [38]. The porous structure of MIL-88b is an organic-inorganic network with rhombic and hexagonal cavities, in the nodes of which iron oxo clusters are evenly distributed [39–41]. Electron-rich organic terephthalic acid ligands included in the MIL-88b structure typically act as electron donors for the reduction of Fe(III) to Fe(II) [42]. It is also known that MIL-88b does not have sufficient chemical stability [43], but this fact is even useful for the sacrificial release of iron ions during the Fenton process [44].

The combination of MOFs with magnetic particles (MPs) is considered more promising, as it offers the potential to combine the advantageous properties of both MOFs and MPs. This could result in enhanced chemical stability of the material and the additional possibility of precise positioning with rapid and easy release under the influence of an external magnetic field [45, 46]. A comprehensive examination of the Fenton reactivity of diverse iron-based materials can be found in the existing literature. It is observed that the most significant factors determining the reaction rate are crystallinity, specific surface area, oxygen vacancies and valence states of iron, as well as the redox potential of the transformation reaction Fe^{3+}/Fe^{2+} [6, 21, 22, 37, 47]. However, there is currently no effective tool based on machine learning methods that can be used to predict the catalytic activity of iron-containing materials in the processes of decomposition of organic pollutants using the Fenton reaction.

In this study, a predictive model based on multivariate correlation analysis was proposed to enable the prediction of the effectiveness of the pro-oxidant properties of the resulting iron-containing materials. The concentration of methylene blue (MB) after decomposition is considered as an indicator of the rate of the Fenton reaction. The scientific novelty of this study also lies in the preparation of iron-containing Fe-MOFs magnetic composites with enhanced pro-oxidant properties for inducing ROS under model conditions due to additional functionalization of the structure with humic acids (HA) or ascorbic acid (AA) as chelating agents. It is known that HA, which is part of the magnetically active catalyst, also serves as a stabilizer of magnetite nanoparticles (NP) [48]. In addition, magnetite NP modified with HA or AA exhibit anti/pro-oxidant properties due to the presence of donor-acceptor groups. Therefore, in this paper MOF and silane-based composites (in particular, tetraethoxysilane and 3-aminopropyltriethoxysilane copolymer, TA) containing magnetite (Fe_3O_4) or maghemite (γ-Fe_2O_3), as well as the stabilizer HA/prooxidant AA were synthesized and tested in the decomposition reaction of MB. We think that this study can clarify the structure-activity relationships of different iron minerals in heterogeneous Fenton processes and inspire the development of new heterogeneous Fenton catalysts based on MOFs and silanes.

Experimental

Synthesis Fe-MOFs Composites

In this study, a rational method for the synthesis of **MOFs** was used to target iron-carboxylate MOFs such as MIL-88b [49]. To synthesize the coordination polymer of the MIL-88b series, 5 g of terephthalic acid and 7.35 g of Fe_3OAcetate were dissolved in 100 mL of dimethylformamide with stirring on a magnetic stirrer (300 rpm) for 30 min. Fe_3OAcetate ($[Fe_3O(C_8H_4O_4)_3(H_2O)_3]Cl$) was synthesized according to a previously published method [43]. The resulting composites were isolated using a Buchner funnel, washed multiple times with distilled water subsequently, and dried in a vacuum (10^{-3} Torr, 50 °C, 12 h). The yield was 6.82 g.

In a typical synthesis of a series of such composites, Fe^{2+} to Fe^{3+} chlorides were added at a rate to produce magnetite of 25 wt % in the final composite (**MOF-Fe_3O_4**). At the first stage, the synthesis of magnetite was carried out according to the Elmore method [50]. Then, terephthalic acid and Fe_3OAcetate were added to the resulting reaction mixture. The synthesis was maintained with constant stirring at 900 rpm in an argon atmosphere for 60 min. The remaining steps, including precipitation and purification, were similar to those used in the preparation of MOFs. The yield was 4.6 g.

The **MOF-HA-Fe_3O_4** or **MOF-AA-Fe_3O_4** complex was prepared in a manner similar to MOF-Fe_3O_4, with the addition of HA or AA after the magnetite or maghemite suspension preparation stage. The amount added of AA and HA was 200 mg (10 wt % based on MOF). At the first stage, the synthesis of magnetite was carried out according to the Elmore method [50]. Then 200 mg of the stabilizer HA or pro-oxidant AA was added to the reaction system and the resulting mixture was kept for 5 min with stirring 800–1200 rpm at the pH≈7. Subsequently, terephthalic acid ($C_8H_6O_4$, 1.4 g, 0.084 mol) and Fe_3OAcetate (2.07 g, 0.0028 mol) were added to the resulting reaction mixture for *in situ* synthesis MOF. The reaction mixture was maintained under stirring (800–1200 rpm) on an overhead stirrer for 60 min. The remaining steps, including precipitation and purification, were similar to those used in the preparation of MOF. The yield was 4.5 and 3.5 g for MOF-HA-Fe_3O_4 and MOF-AA-Fe_3O_4 respectively.

Synthesis Fe-TA Composites

The **TA** is a silica gel functionalized with 3-aminopropyl fragments obtained by the interaction of tetraethoxysilane (T) and 3-aminopropyltriethoxysilane (A). To obtain TA, 10 mL of tetraethoxysilane and 4.2 mL of 3-aminopropyltriethoxysilane (T:A ratio = 1:0.5, mol/mol) were mixed with 150 mL of deionized water. The mixture was continuously stirred on an overhead stirrer (600 rpm, for 10 min) and then shaken on a laboratory shaker (150 rpm, for 24 h) at room temperature. The resulting precipitate was washed with distilled water pH~8 and centrifuged (3000 rpm, 10 min, 4 cycles). The sample was lyophilized and dried in a freeze dryer at –37 °C. The yield was 4.57 g.

In order to obtain the **TA-HA-Fe^{3+}** (1:0.1:0.5 wt/wt/wt), complex (1:0.1:0.5 wt/wt/wt), the iron salts were weighed based on the amount of Fe in 1 g of magnetite per 2 g of TA. Portions of 1.562 g $FeCl_3 \cdot 6H_2O$ and 0.2 g HA (sodium salt of humic acids, Powerhumus, Humintech, Germany; 5 $mmol \cdot g^{-1}$ of COOH and OH-groups, Mw=8 kD) were weighed and dissolved in 200 mL of deionized water. The solution was then dispersed in an ultrasonic bath for 10 min. Subsequently the TA particles were poured into the solution and redispersed in an ultrasonic bath for 10 min. The solutions were stirred on a laboratory shaker (170 rpm) for 18 h. The resulting precipitate was separated using a centrifuge (3000 rpm, 10 min) and dried in air at room temperature. The yield was 2.7 g.

The preparation of magnetically active **TA-HA-Fe_2O_3** (1:0.1:0.5, wt/wt/wt) composites was carried out in several stages. For this purpose, 2 g of TA and 0.2 g of HA were mixed with 200 mL of degassed distilled water in a non-inert atmosphere. The mixture was stirred at 1400–1500 rpm for 30 min. Then, weighed amounts of salts were added: 2.7 g of $FeCl_3 \cdot 6H_2O$, 0.99 g $FeCl_2 \cdot 4H_2O$ and 6 mL 25 % NH_4OH, calculated per 1 g of Fe_3O_4. The mixture was stirred at 1400–1500 rpm for 10 min. The remaining stages, including precipitation and purification, were similar to those used in the preparation of TA-HA-Fe^{3+}. The yield was 2.85 g.

The **TA-AA-Fe_3O_4** (1:0.1:0.5 wt/wt/wt) complex was obtained by following the same procedure as that used for the synthesis of the TA-HA-Fe_3O_4, with the exception that the same amount of AA was added instead of HA. The salt samples were dissolved in degassed distilled water in an argon atmosphere at 1400–1500 rpm. Then 6 m 25 % NH_4OH were added and stirred for 30 min. The resulting Fe_3O_4 precipitate was separated using a magnet (0.3 T) and washed once with 200 mL of degassed distilled water. Then AA was dissolved in 70 mL of a solution containing magnetite, 200 mL of 96 % C_2H_5OH (pH=7-8) were added with constant stirring (1200 rpm) and 2 g of TA. The solution was stirred on an overhead stirrer (1000 rpm) for 60 min. The remaining steps, including precipitation and purification, were similar to those used in the preparation of MOFs. The yield was 2.66 g.

X-ray Diffraction Analysis (XRD)

The phase composition and primary particle size of the samples were determined by XRD analysis using the Bragg-Brentano geometry on a Philips X'Pert diffractometer (Philips Analytical, Eindhoven, The Netherlands). Cu-K_α radiation (λ = 1.5406 Å) was used as the X-ray source. The collected data were smoothed using the Savitzky-Golay algorithm [51]. The measurements were performed at room temperature, covering an angular range of $10° < 2\Theta < 110°$ with a step size of 0.025° and a dwell time of 1 second per step.

Low-Temperature Nitrogen Adsorption Analysis

The specific surface area and porous structure characteristics of the samples were determined by N_2 adsorption-desorption analysis using a Quantachrome instrument. Prior to analysis, the samples were degassed and subjected to vaporization. They were then "thermally trained" by heating in a stream of inert N_2 gas under vacuum at 150 °C for 30 min. The adsorption isotherms were obtained by measuring the volume of N_2 gas adsorbed by the sample surface as a steady flow of a He-N_2 gas mixture with varying N_2 concentration (0 to approximately 1 volume fraction) was passed through the sample at liquid nitrogen temperature (77 K).

Desorption isotherms were obtained by measuring the volume of N_2 desorbed from the sample surface as the N_2 concentration in the gas mixture was decreased from approximately 1 to 0 volume fraction. The specific surface area and characteristics of the porous structure were calculated from the obtained adsorption-desorption isotherms using the Brunauer-Emmett-Teller (BET) and Barret-Joyner-Halenda (BJH) methods.

Elemental Analysis

The content of C, H, N was determined on an elemental analyzer "VarioMicrocube" (ElementarGmbH, Germany) using the classical Dumas-Preglia method — by burning the sample in the presence of an oxidant in an inert gas current. The Fe content was determined on the atomic absorption spectrometer "AAS-3" (Zeiss, Germany). The identification of functional groups of the obtained compounds was carried out on a Perkin-Elmer Spectrum 100 Fourier transform infrared spectrometer (USA, 2006) equipped with an attachment for broken total internal reflection (TIR) with a diamond prism of single reflection. The penetration depth for a medium with a sufficiently deep refractive index (2.43) at 1000 cm^{-1} is 1.66 microns. FT-IR-ATR spectra were taken in the range of 360–4000 cm^{-1} at room temperature using 24 scans and a resolution of 2 cm^{-1}. The baseline of the obtained spectra was corrected in the OPUS program.

X-ray Photoelectron Spectroscopy (XPS)

The surface layer of the samples was investigated by X-ray photoelectron spectroscopy. The XPS system was equipped with a dual anode (Al, Mg) X-ray source (SPECS XR50) and a hemispherical analyzer (SPECS Phoibos 150). The measurements were performed using Al K-α radiation (excitation energy: 1486.61 eV). The XPS data were analyzed using the CasaXPS software package. The peaks were deconvoluted using a Shirley-type background and a combination of Gaussian (50 %) and Lorentzian (50 %) functions. The half-heights of the C1s and O1s peaks were recorded during the analysis.

Dynamic and Electrophoretic Light Scattering (DLS, ELS)

The surface charge of the NPs, known as the zeta potential, was determined using ELS. This analysis was performed on a NanoBrook Omni particle analyzer (Brookhaven Instruments Corporation, Holtsville, NY, USA) at a specific wavelength of 633 nm. The instrument uses a solid-state He-Ne laser as a light source and measures scattered light at an angle of 173 degrees. All measurements were performed at a controlled temperature of 25 °C. Prior to analysis, each sample was diluted to a concentration of 0.1 g L^{-1} with an appropriate solvent. A standardized procedure was followed to ensure consistent measurement conditions. The diluted sample was dispersed in an ultrasonic bath for 10 seconds to break up any particle aggregates. After dispersion, the sample was allowed to rest for a further 100 seconds to reach equilibrium prior to measurement. All measurements were performed at a controlled temperature of 25±0.1 °C to minimize thermal fluctuations and ensure reproducibility. The pH of the suspension was adjusted to a range of 3 to 10 using either dilute NaOH or HCl. The pH was measured using a combination pH electrode for accurate control.

The results of the studies are presented in Table 1.

Table 1

Physicochemical characteristics of composites

Sample	Lattice parameter[a]	SSA[b]	Elemental analysis data	XPS data[c]	Zeta potential[d]	References
	Å	$m^2 g^{-1}$	Fe, %	Fe^{2+}/Fe^{3+}	mV	
MOF	–	220	18.5	0.66	–8.0	[44]
MOF-Fe_3O_4	8.378	197	33.9	1.02	+4.7	[44]
MOF-HA-Fe_3O_4	8.387	83	43.2	–	–9.1	–
MOF-AA- Fe_3O_4	8.389	174	44.4	1.59	–3.2	[44]
TA-HA-Fe^{3+}	–	237	15.8	1.08	–25	–
TA-HA-Fe_2O_3	8.301	208	20.2	–	+29.5	–
TA-AA-Fe_3O_4	8.381	116	32.5	–	–2.5	[52]

Notes: [a]The lattice cell parameter was calculated using XRD data; [b]SSA — specific surface area determined by low-temperature nitrogen adsorption; [c]The Fe^{3+}/Fe^{2+} ratio is calculated using XPS data; [d]Zeta potential determined by ELS at pH=4.6 in deionized water.

Results and Discussion

Evaluation of the Prooxidant Ability of selected Promising Samples in the Fenton Reaction

To evaluate the prooxidant activity of the obtained iron-containing preparations in the Fenton reaction, the well-known reaction of decolorization of MB in the presence of hydroxyl radicals •OH was used. The hydroxyl radicals as a result of the disproportionation reaction of 100 mM H_2O_2, catalyzed by selected promising NP, at pH 4.5, close to the pH of the tumor [53], and 37 °C, lead to the discoloration of the MB solution to colorless cation-free MB. The rate of bleaching of MB was assessed 0, 30, 90 and 180 min after preparation of the suspension by the change in optical density at a wavelength of 652 nm using UV-Vis-spectroscopy. The interaction of MB with iron-containing compounds can be described by three processes occurring both in parallel and sequentially: (1) sorption of MB on the surface of NP, (2) photodegradation of MB, and (3) degradation of MB in the presence of H_2O_2 as a result of the Fenton reaction. Hernandez et al. [54] showed that sorption and photodegradation of MB can be considered as two sequential processes, at the same time, 150 min after the start of interaction of the dye with magnetite NP, the concentration of MB in the supernatant decreases by half from 20 to 10 mg L^{-1}. This was attributed by the authors to photodegradation of the product as determined by mass spectrometry. Hydrogen peroxide was then added to initiate the Fenton reaction, which would increase the rate of dye decomposition. However it is difficult to estimate the concentration of MB undergoing separate sorption or photodegradation or degradation during the Fenton reaction due to the complexity of the processes occurring, a comparison was conducted between the rate of change in the optical density of the solution in the presence/absence of H_2O_2 (during sorption/degradation during the Fenton reaction).

An assessment of the degradation of MB in sorption experiments (in the absence of H_2O_2) and the Fenton reaction (in the presence of H_2O_2) showed that all preparations, with the exception of TA-AA-Fe_3O_4, demonstrate a decrease in MB concentration by 60 % or more within 180 min (Fig. 1*a*).

The insufficient activity of the TA-AA-Fe_3O_4 sample can probably be associated with the low concentration of both released ions Fe^{3+} and Fe^{2+} (Fig. 1*b*, *c*). Thus, the TA-AA-Fe_3O_4 sample is considered unpromising and is excluded from further sampling.

The next step is to assess the role of the Fenton reaction as a source of hydroxyl radicals in the reduction of the MB in the supernatant. In Figure 2 shows the difference between the concentrations of MB subjected to sorption and decomposition under the influence of H_2O_2 for the remaining four promising samples.

The data obtained indicates that, the decrease in the concentration of MB in the supernatant for the MOF-HA-Fe_3O_4 sample is a result of the sorption processes, rather than the Fenton reaction. This observation leads to the conclusion that the MOF-HA-Fe_3O_4 sample can be excluded from the list of promising samples. The high sorption capacity of MOF-HA-Fe_3O_4 is probably due to the presence of HA in its composition together with MOF. One can assume a competitive mechanism of sorption and degradation, as a result of which sorption processes occur faster due to the greater availability of MB in solution.

At the next stage, the evaluation of promising samples was carried out based on the reaction rate and reaction rate constant. Thus, an assessment of the reaction rate showed that the preparations TA-HA-Fe_2O_3 and TA-HA-Fe^{3+} demonstrate a maximum reaction rate (both sorption and Fenton reaction) 30 min after the start of the experiment, while the reaction in the presence of MOF-AA-Fe_3O_4 reaches its maximum 90 min after the start of the experiment, indicating a prolonged effect of the NP. A comparison shows that the rate of the Fenton reaction decreases in the series: TA-HA-Fe^{3+} > MOF-AA-Fe_3O_4 > TA-HA-Fe_2O_3. This correlates with the release patterns of both Fe^{3+} and Fe^{2+}: TA-HA-Fe^{3+} and TA-HA-Fe_2O_3 released 9 % and 0.1 % Fe^{3+} after 30 min, while the concentration of Fe^{2+} released by the MOF-AA-Fe_3O_4 only increased within three hours and reached 0.45 %.

The pronounced activity of the TA-HA-Fe^{3+} sample is associated with the release of Fe^{3+} from the complex, the rate of which is higher than that of samples with iron oxide NP. This is consistent with the results of Wang et al. [55] who found that at low pH values (pH < 4.2), iron ions Fe(II, III) released from the complexes predominantly participate in the formation of •OH hydroxyl radicals salts, while at neutral pH values the formation of •OH occurs mainly due to the catalytic decomposition of H_2O_2 by surface iron (which is at least 50 times more effective than dissolved iron ions) [56], which determines the choice of NP as ion sources gland. At the same time, [57, 58] found that the rate of generation of •OH radicals using free Fe^{2+} is higher than with the participation of Fe^{2+} on the surface of Fe_3O_4 NP.

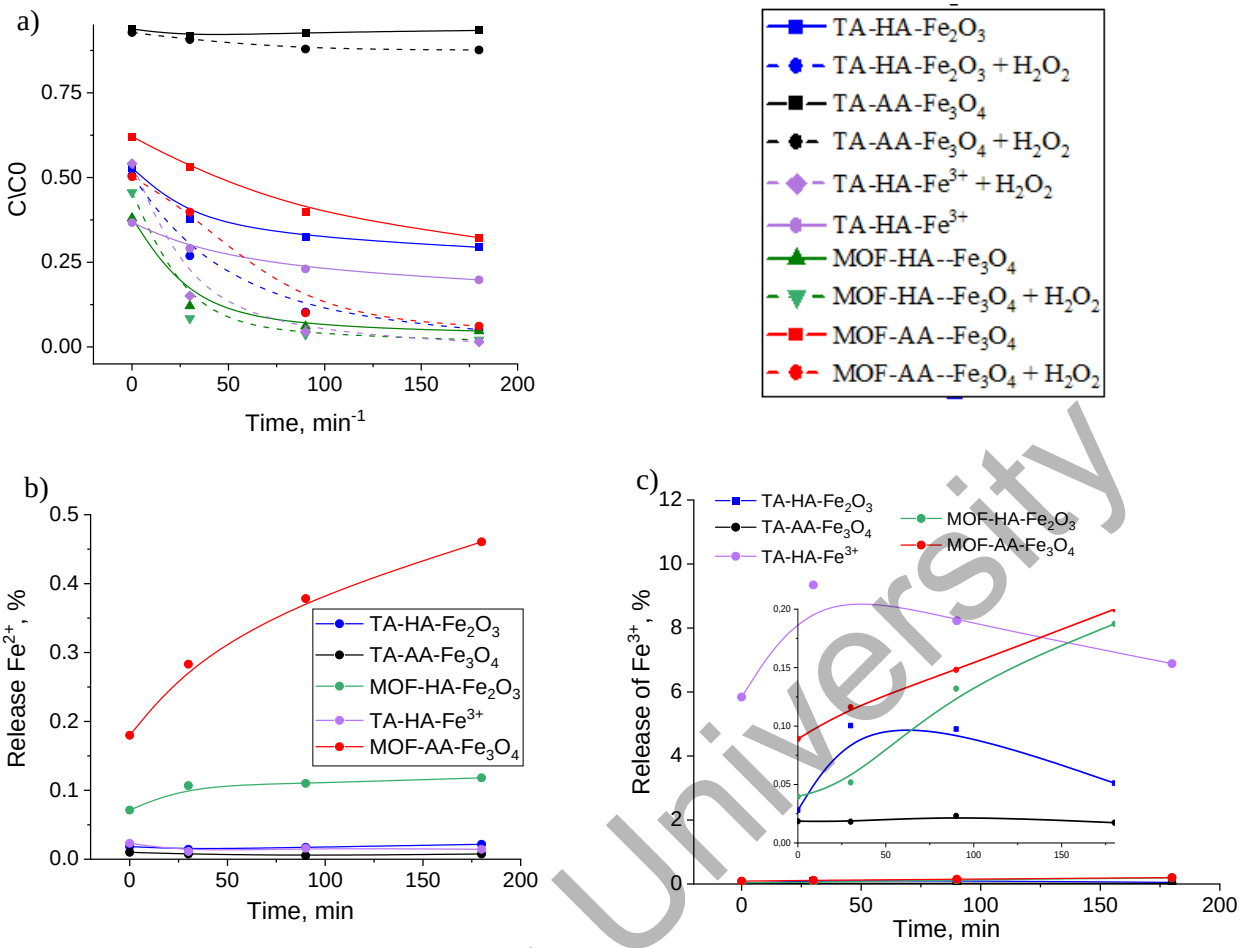

Figure 1. (*a*) Catalytic degradation of MB by samples (MB concentration = 11 mg L^{-1}; H_2O_2 concentration = 100 mM; and sample dosage = 1 g L^{-1}, 0.1 M NaAc buffer pH = 4.5; 37 °C). Solid lines show MB adsorption without H_2O_2; dotted lines show a decrease in the MB concentration with H_2O_2. (*b*) Kinetics of the Fe^{2+} release. (*c*) Kinetics of the Fe^{3+} release. Data normalized to the iron content

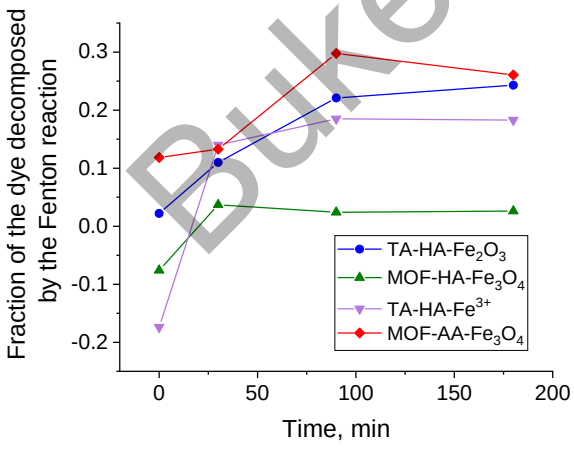

Figure 2. Fraction of the dye decomposed by the Fenton reaction for the four perspective samples

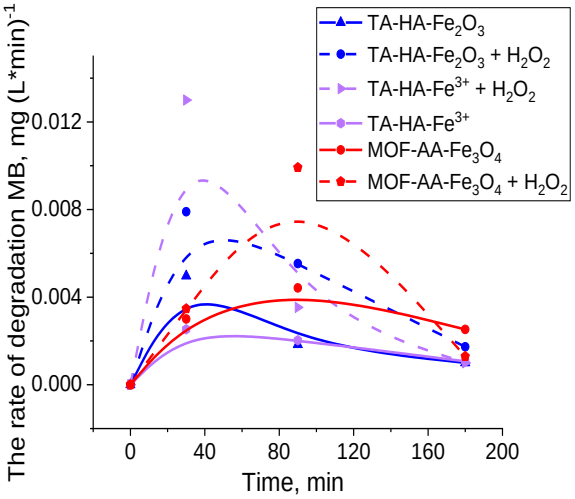

Figure 3. The rate of decomposition of MB versus time

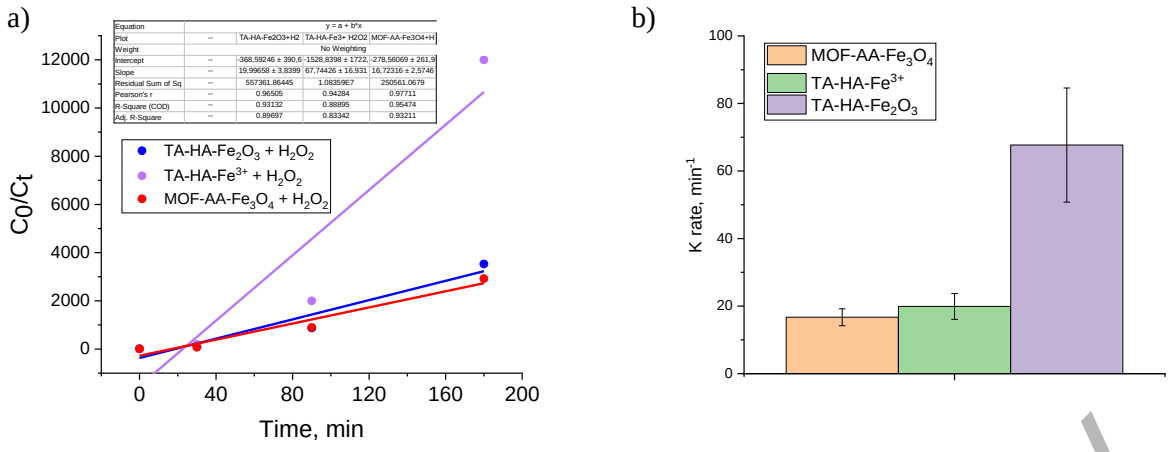

Figure 4. (*a*) Kinetic curve of pseudo-second-order MB degradation and values of degradation rate constants (0.1 M NaAc buffer pH=4.5; 100 mM H_2O_2; 0-180 min; 37 °C; concentration of NPs=10 g L^{-1}; concentration of MB=11 mg L^{-1}) (*b*) Constants of the reaction's rate

An assessment of the reaction rate kinetics showed that the Fenton reactions in the presence of three promising samples can be classified as pseudo-second order reactions (R^2 values are presented in the table) with rate constants of 16.7±2.5 s^{-1}, 19.9±3.8 s^{-1} and 67.7±19.3 s^{-1} for MOF-AA-Fe_3O_4, TA-HA-Fe_2O_3 and TA-HA-Fe^{3+}, respectively (Fig. 4*a*, *b*). It is obvious that the highest value of the reaction rate constant in the presence of TA-HA-Fe^{3+} is due to the highest rate of release of Fe^{3+}.

Regression Models

In order to comprehend the mechanism through which the nature of NP exerts its influence on their pro-oxidant properties, a predictive model was constructed on the basis of a multivariate correlation analysis of the relationship between "physicochemical properties and concentration of MB after degradation". The presence of iron ions is the most obvious catalyst for the Fenton reaction, however our objective was to ascertain whether other physicochemical characteristics of the samples would affect the rate of the Fenton reaction. In this case, the concentration of MB after degradation is an indicator of the rate of the Fenton reaction, and therefore the effectiveness of the pro-oxidant properties of the resulting samples. The initial concentration of iron in the preparation, the unit cell parameter (for oxides), the ratio of Fe^{2+}/Fe^{3+} on the surface, specific surface area, zeta potential, and the concentration of released Fe^{2+} and Fe^{3+} were used as physicochemical characteristics. At the first stage, a regression model was built to assess the influence of selected six parameters (initial iron concentration, unit cell parameter, ratio of Fe^{2+}/Fe^{3+} on the surface, specific surface area, zeta potential, concentration of released Fe^{2+} and Fe^{3+} in total) on the concentration of MB for five promising samples, as well as MOF and Fe_3O_4-MOF which had been previously studied. The zeta potential parameters and the concentration of the released Fe^{2+} and Fe^{3+}, as well as the concentration of MB after the Fenton reaction, were selected as the initial experimental variables and were observed over a five-minute period.

An assessment of the coefficient of determination (adjusted R^2 = 0.9343) and p-value = 0.0433 shows that a linear model can be used to describe the dependence of the result (MB concentration) on the output parameters. The adjusted R^2 value indicates that the linear model can account for more than 93 % of the total variability while the remaining values cannot be described by it.

The results of an analysis based on the methodology of surface response made it possible to compose the following second order equation:

$$Y = 0.0995 + 0.0063\ A + 0.0314\ B - 0.1338\ C + 0.151125\ D - 0.0109\ F - 0.0591\ E,$$

where Y is the concentration of MB in the Fenton reaction (mg L^{-1}), A is the initial concentration of iron in the sample (%), B is the unit cell parameter (A), C is the ratio of Fe^{2+}/Fe^{3+} on the surface of the sample, D is the total concentration of released iron ions (Fe^{2+} and Fe^{3+}, %), F is the specific surface area (m^2 g^{-1}), E is surface charge (mV).

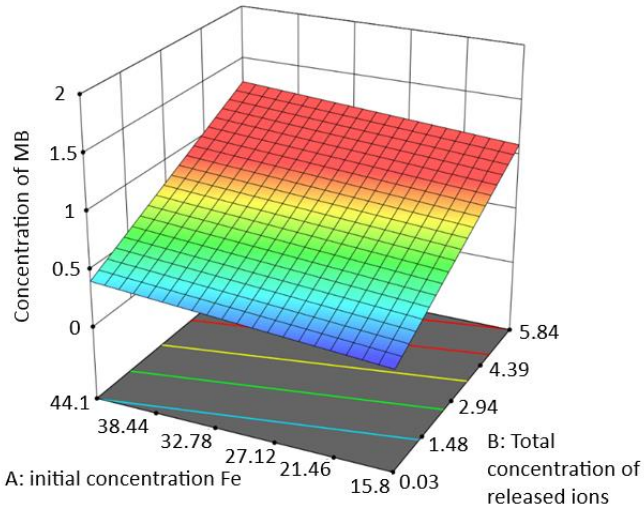

Figure 5. Effect of initial iron concentration and total concentration of released Fe^{2+}/Fe^{3+} on MB degradation

The equation permitted the evaluation of the influence of a particular factor and the interaction between the six factors on the concentration of MB. The sign of the coefficient in the equation indicates the direction of the trend in the results: negative and positive coefficients show negative and positive effects, respectively. A positive sign and therefore a positive effect indicate that the response changes in direct proportion to a change in the level of the factor, and a negative effect with an inverse change in the level of the factor. As evidenced by the derived equation (1), the effects of A, B and D on the concentration of MB are positive, whereas those of C, F and E are negative. However, the p-value indicates that only the total concentration of released iron ions is a significant factor (p-value = 0.0162, parameters with a p-value < 0.05 are considered significant, Fig. 5). Thus, the concentration of released iron ions is the only parameter selected that affects the kinetics of the Fenton reaction.

It was of interest to evaluate the influence of separately Fe^{2+} and Fe^{3+} and reaction time on the kinetics of the Fenton reaction. To this end, a regression model was also built with three parameters (reaction time, concentration of released Fe^{2+} and concentration of released Fe^{3+}) and response (concentration of MB in the supernatant after the Fenton reaction). The predicted R^2 value of 0.7800 is in the agreement with the adjusted R^2 value of 0.9111 with a difference of less than 0.2. Adeq Precision, indicating the signal-to-noise ratio, is 17.702, which is significantly greater than 4, indicating adequate signal and the ability to use the model to predict the kinetics of the Fenton reaction (Fig. 6). The model's F-value of 31.89 and p-value < 0.0001 indicate that the model is significant. There is only a 0.01 % chance that such a large F value could arise from noise. Furthermore, there is a strong correlation between the predicted and experimental values.

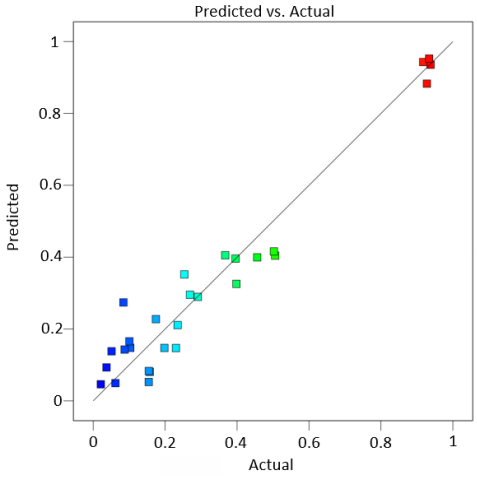

Figure 6. Dependence of predicted values on predicted values

Based on the obtained coefficients, a quadratic regression equation was compiled:

$$Y = -2.24626 - 0.1317\,A - 2.7981\,B - 2.5506\,C - 0.0832\,AB + 0.0779\,AC - 2.928\,BC + 0.1318\,A^2 + 0.1392\,B^2 - 0.1642\,C^2,$$

where Y is the concentration of MB in the Fenton reaction (%), A is the reaction time (min), B is the concentration of released Fe^{2+} (%), C is the concentration of released Fe^{3+} (%).

According to the p-value parameters (Table 2), the concentrations of released iron ions, the square of the Fe^{2+} ion concentration, and the product of the reaction time and the Fe^{3+} concentration are statistically significant.

Table 2

Data of ANOVA for quadratic model

Source	Sum of Squares	df	Mean Square	F-value	p-value	
Model	2.11	9	0.2342	31.89	< 0.0001	significant
A-Time	0.0244	1	0.0244	3.33	0.0848	
B-Fe^{2+}	0.0627	1	0.0627	8.54	0.0091	
C-Fe^{3+}	0.0486	1	0.0486	6.61	0.0192	
AB	0.0107	1	0.0107	1.46	0.2425	
AC	0.0206	1	0.0206	2.81	0.1111	
BC	0.0662	1	0.0662	9.01	0.0077	
A^2	0.0743	1	0.0743	10.12	0.0052	
B^2	0.0200	1	0.0200	2.72	0.1163	
C^2	0.0183	1	0.0183	2.49	0.1323	
Residual	0.1322	18	0.0073			
Cor Total	2.24	27				

Comparison of the sign and magnitude of the coefficients shows that an increase in ion concentration leads to a decrease in the concentration of MB. This implies that the rate of the Fenton reaction increases, with the concentration of Fe^{2+} exerting a greater influence than Fe^{3+}. This is consistent with the fact that the Fenton reaction initiated by Fe^{2+} is significantly faster ($k = 63\ M^{-1}\cdot S^{-1}$) than the reaction occurring during the reduction of Fe^{3+} to Fe^{2+} ($k = 0.001–0.02\ M^{-1}\cdot S^{-1}$) [36]. Notably, the effect of time on the reaction is indirect, and occurs in combination with the concentration of Fe^{3+}.

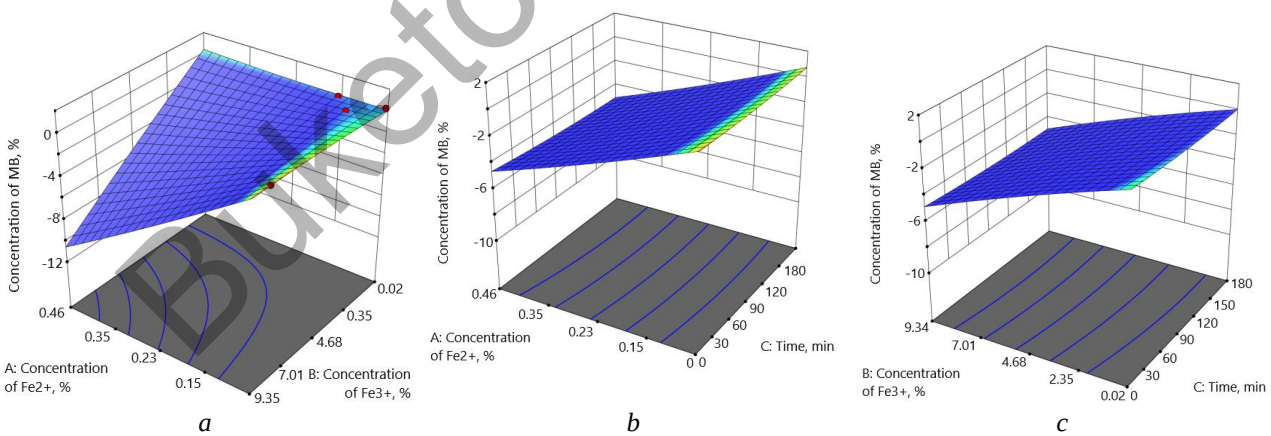

Figure 7. Response surfaces for the MB degradation value for different combinations of factors: concentration of released Fe^{3+} and Fe^{2+} (*a*), concentration of released Fe^{2+} and time (*b*) and concentration of released Fe^{3+} and time (*c*)

It can be demonstrated that the maximum reaction rate can be achieved at different times by controlling the concentration of released iron ions. For example, in some cases, a rapid effect of the sample in the first minutes of its administration is required. Then, to achieve the maximum effect (MB concentration in the supernatant should be 0 % 5 min after administration), 0.13 % Fe^{2+} and 1.78 % Fe^{3+} are required (Fig. 7*a*). Therefore, if we assume that the relationship between the concentration of the initial sample and the ions re-

leased by it is linear, then using the MOF-AA-Fe_3O_4 sample as an example, to achieve the maximum reaction rate in 5 min, it is necessary to introduce 47.6 g L^{-1} of the sample. On the other hand, when the concentration of released Fe^{2+} is reduced to 0.12 %, the concentration of Fe^{3+} released to degrade the entire MB within 5 min is 1.41 % (Fig. 7*c*). Thus, the use of TA-HA-Fe^{3+} would allow achieving such a reaction rate using only 1.6 g L^{-1} of the sample. Thus, it is more rational to use the sample MOF-AA-Fe_3O_4 to achieve a prolonged prooxidant effect 3 h after insertion, and TA-HA-Fe^{3+} to achieve its maximum effect within the first 30 min after insertion.

To test the model, samples of MOF, MOF-Fe_3O_4, Fe_3O_4-MOF [43, 44] and Fe_3O_4-SiO_2 were selected and the degradation of methylene blue, as well as the release of Fe^{2+} and Fe^{3+} 60 minutes after the start of the experiment, were assessed (Supplementary Materials, Table S1, Fig. S1). The experimental data values correlate with the theoretical ones, the value of the corrected determination coefficient R^2 was 0.87. Thus, the obtained model can be successfully used to predict the degradation of methylene blue in kinetic experiments based on the concentration of released Fe^{2+} and Fe^{3+} ions. The limitation is the difficulty in extrapolating the model when using data that are outside the ranges of the input parameters.

Conclusions

This paper presents the synthesis and testing of composites containing the metal-organic framework MIL88b(Fe), as well as nanoparticles of magnetite (Fe_3O_4) or maghemite (γ-Fe_2O_3) modified by humic acids or ascorbic acid in the decomposition reaction of methylene blue. The proposed predictive model based on multi-factor correlation analysis of "physical-chemical properties — methylene blue concentration after degradation" showed that in a line of selected parameters (initial iron concentration in sample, elemental cell parameter, Fe^{2+}/Fe^{3+} ion ratio on sample surface, total iron ion released concentration, surface area specific, surface charge), a significant factor influencing Fenton reaction kinetics, is only the total concentration of the released iron ions (p-value = 0.0162). Evaluation of the influence of separate Fe^{2+} and Fe^{3+} ions and reaction time to the Fenton reaction kinetics by multi-factor analysis showed that concentrations of released iron ions are statistically significant, with the concentration of Fe^{2+} ions affecting more than Fe^{3+}. The developed model is proposed for forecasting the prooxidant properties of preparations.

Supporting Information

The Supporting Information is available free at https://ejc.buketov.edu.kz/index.php/ejc/article/view/141/101

Funding

This research was supported by the Russian Science Foundation (project № 22-73-10222).

*Author Information**

**The authors' names are presented in the following order: First Name, Middle Name and Last Name*

Daniel Saman — MD Student, Moscow Aviation Institute (National Research University), 125993, Moscow, Russia; e-mail: saman_d@mail.ru

Lyubov Sergeevna Bondarenko (*corresponding author*) — Candidate of Chemical Sciences, Associate Professor, Department 903 "Advanced Materials and Technologies for Aerospace Engineering", Moscow Aviation Institute (National Research University), 125993, Moscow, Russia; e-mail: l.s.bondarenko92@gmail.com; https://orcid.org/0000-0002-3107-0648

Rose Kurmangalievna Baimuratova — Candidate of Chemical Sciences, Junior Researcher, Federal Research Center of Problems of Chemical Physics and Medicinal Chemistry, Russian Academy of Sciences, 142432, Chernogolovka, Moscow region, Russia; e-mail: roz_baz@mail.ru; https://orcid.org/0000-0002-8389-6871

Artur Albertovich Dzeranov — 4th year PhD Student, Department 903 "Advanced Materials and Technologies for Aerospace Applications", Moscow Aviation Institute (National Research University), 125993, Moscow, Russia; e-mail: arturdzeranov99@gmail.com; https://orcid.org/0000-0003-3240-9321

Gulzhian Iskakovna Dzhardimalieva — Doctor of Chemical Sciences, Head of Laboratory of Metallopolymers, Federal Research Center of Problems of Chemical Physics and Medicinal Chemistry, Russian

Academy of Sciences, Chernogolovka, Moscow region, 142432, Russia; e-mail: dzhardim@icp.ac.ru; https://orcid.org/0000-0002-4727-8910

Nataliya Sergeevna Tropskaya — Doctor of Biological Sciences, Head of the Department of Experimental Damage Laboratory, Sklifosovsky Research Institute for Emergency Medicine, 129090, Moscow, Russia; e-mail: ntropskaya@mail.ru; https://orcid.org/0000-0001-5870-9483

Kamila Asylbekovna Kydralieva — Doctor of Chemical Sciences, Department 903 "Advanced Materials and Technologies for Aerospace Applications", Moscow Aviation Institute (National Research University), 125993, Moscow, Russia; e-mail: kydralievaka@mai.ru; https://orcid.org/0000-0002-4596-4140

Author Contributions

The manuscript was written through contributions of all authors. All authors have given approval to the final version of the manuscript. CRediT: **Daniel Saman** — investigation; **Lyubov Sergeevna Bondarenko** — methodology, validation, writing-original draft, writing-review & editing; **Rose Kurmangalievna Baimuratova** writing-original draft, — investigation; **Artur Albertovich Dzeranov** — investigation; **Gulzhian Iskakovna Dzhardimalieva** — data curation, conceptualization; **Nataliya Sergeevna Tropskaya** — formal analysis, resources; **Kamila Asylbekovna Kydralieva** — data curation, conceptualization, writing-original draft, writing-review & editing.

Acknowledgments

Low-temperature nitrogen adsorption were carried out in accordance with the state tasks, state registration 124013000757-0 using the equipment of the Multi-User Analytical Center of FRC PCP and MC RAS.

Conflicts of Interest

The authors declare no conflict of interest.

References

1 Jain, B., Singh, A. K., Kim, H., Lichtfouse, E., & Sharma, V. K. (2018). Treatment of organic pollutants by homogeneous and heterogeneous Fenton reaction processes. *Environmental Chemistry Letters*, *16*(3), 947–967. https://doi.org/10.1007/s10311-018-0738-3

2 Sreeja, P. H., & Sosamony, K. J. (2016). A Comparative Study of Homogeneous and Heterogeneous Photo-fenton Process for Textile Wastewater Treatment. *Procedia Technology*, *24*, 217–223. https://doi.org/10.1016/j.protcy.2016.05.065

3 Clarizia, L., Russo, D., Di Somma, I., Marotta, R., & Andreozzi, R. (2017). Homogeneous photo-Fenton processes at near neutral pH: A review. *Applied Catalysis B: Environmental*, *209*, 358–371. https://doi.org/10.1016/j.apcatb.2017.03.011

4 Wang, C., Liu, H., Sun, Z., Huang, J., & Liao, Y. (2012). Supported Nanosized α-FeOOH Improves Efficiency of Photoelectro-Fenton Process with Reaction-Controlled pH Adjustment for Sustainable Water Treatment. *International Journal of Photoenergy*, *2012*, 1–7. https://doi.org/10.1155/2012/689807

5 Kremer, M. L. (2003). The Fenton Reaction. Dependence of the Rate on pH. *The Journal of Physical Chemistry A*, *107*(11), 1734–1741. https://doi.org/10.1021/jp020654p

6 Nidheesh, P. V. (2015). Heterogeneous Fenton catalysts for the abatement of organic pollutants from aqueous solution: A review. *RSC Advances*, *5*(51), 40552–40577. https://doi.org/10.1039/C5RA02023A

7 Litter, M. I., & Slodowicz, M. (2017). An overview on heterogeneous Fenton and photoFenton reactions using zerovalent iron materials. *Journal of Advanced Oxidation Technologies*, *20*(1), 20160164. https://doi.org/doi:10.1515/jaots-2016-0164

8 Hussain, S., Aneggi, E., & Goi, D. (2021). Catalytic activity of metals in heterogeneous Fenton-like oxidation of wastewater contaminants: a review. *Environmental Chemistry Letters*, *19*(3), 2405–2424. https://doi.org/10.1007/s10311-021-01185-z

9 Azfar Shaida, M., Verma, S., Talukdar, S., Kumar, N., Salim Mahtab, M., Naushad, Mu., & Haq Farooqi, I. (2023). Critical analysis of the role of various iron-based heterogeneous catalysts for advanced oxidation processes: A state of the art review. *Journal of Molecular Liquids*, *374*, 121259. https://doi.org/10.1016/j.molliq.2023.121259

10 Li, N., He, X., Ye, J., Dai, H., Peng, W., Cheng, Z., Yan, B., Chen, G., & Wang, S. (2023). H2O2 activation and contaminants removal in heterogeneous Fenton-like systems. *Journal of Hazardous Materials*, *458*, 131926. https://doi.org/10.1016/j.jhazmat.2023.131926

11 Zhu, Y., Xie, Q., Deng, F., Ni, Z., Lin, Q., Cheng, L., Chen, X., Qiu, R., & Zhu, R. (2023). The differences in heterogeneous Fenton catalytic performance and mechanism of various iron minerals and their influencing factors: A review. *Separation and Purification Technology*, *325*, 124702. https://doi.org/10.1016/j.seppur.2023.124702

12 Pereira, M. C., Oliveira, L. C. A., & Murad, E. (2012). Iron oxide catalysts: Fenton and Fentonlike reactions — a review. *Clay Minerals*, 47(3). https://doi.org/10.1180/claymin.2012.047.3.01

13 Garrido-Ramírez, E. G., Theng, B. K. G., & Mora, M. L. (2010). Clays and oxide minerals as catalysts and nanocatalysts in Fenton-like reactions—A review. *Applied Clay Science*, *47*(3), 182–192. https://doi.org/10.1016/j.clay.2009.11.044

14 Munoz, M., de Pedro, Z. M., Casas, J. A., & Rodriguez, J. J. (2015). Preparation of magnetite-based catalysts and their application in heterogeneous Fenton oxidation — A review. *Applied Catalysis B: Environmental*, *176–177*, 249–265. https://doi.org/10.1016/j.apcatb.2015.04.003

15 Lai, L., He, Y., Zhou, H., Huang, B., Yao, G., & Lai, B. (2021). Critical review of natural iron-based minerals used as heterogeneous catalysts in peroxide activation processes: Characteristics, applications and mechanisms. *Journal of Hazardous Materials*, *416*, 125809. https://doi.org/10.1016/j.jhazmat.2021.125809

16 Hartmann, M., Kullmann, S., & Keller, H. (2010). Wastewater treatment with heterogeneous Fenton-type catalysts based on porous materials. *Journal of Materials Chemistry*, 20(41). https://doi.org/10.1039/c0jm00577k

17 Jin, Q., Kang, J., Chen, Q., Shen, J., Guo, F., & Chen, Z. (2020). Efficiently enhanced Fenton-like reaction via Fe complex immobilized on silica particles for catalytic hydrogen peroxide degradation of 2,4-dichlorophenol. *Applied Catalysis B: Environmental*, *268*, 118453. https://doi.org/10.1016/j.apcatb.2019.118453

18 González-Bahamón, L. F., Hoyos, D. F., Benítez, N., & Pulgarín, C. (2011). New Fe-immobilized natural bentonite plate used as photo-Fenton catalyst for organic pollutant degradation. *Chemosphere*, 82(8). https://doi.org/10.1016/j.chemosphere.2010.11.071

19 Noorjahan, M., Durga Kumari, V., Subrahmanyam, M., & Panda, L. (2005). Immobilized Fe(III)-HY: An efficient and stable photo-Fenton catalyst. *Applied Catalysis B: Environmental*, *57*(4), 291–298. https://doi.org/10.1016/j.apcatb.2004.11.006

20 Cen, S., Lv, X., Jiang, Y., Fakhri, A., & Gupta, V. K. (2020). Synthesis and structure of iron–copper/hollow magnetic/metal–organic framework/coordination sites in a heterogeneous catalyst for a Fenton-based reaction. *Catalysis Science & Technology*, 10(19). https://doi.org/10.1039/D0CY01027H

21 Cheng, M., Lai, C., Liu, Y., Zeng, G., Huang, D., Zhang, C., Qin, L., Hu, L., Zhou, C., & Xiong, W. (2018). Metal-organic frameworks for highly efficient heterogeneous Fenton-like catalysis. *Coordination Chemistry Reviews*, *368*, 80–92. https://doi.org/10.1016/j.ccr.2018.04.012

22 Lu, S., Liu, L., Demissie, H., An, G., & Wang, D. (2021). Design and application of metal-organic frameworks and derivatives as heterogeneous Fenton-like catalysts for organic wastewater treatment: A review. *Environment International*, *146*, 106273. https://doi.org/10.1016/j.envint.2020.106273

23 Batten, S. R., Champness, N. R., Chen, X. -M., Garcia-Martinez, J., Kitagawa, S., Öhrström, L., O'Keeffe, M., Paik Suh, M., & Reedijk, J. (2013). Terminology of metal–organic frameworks and coordination polymers (IUPAC Recommendations 2013). *Pure and Applied Chemistry*, *85*(8), 1715–1724. https://doi.org/10.1351/PAC-REC-12-11-20

24 Zhang, M., Bosch, M., Gentle Iii, T., & Zhou, H.-C. (2014). Rational design of metal–organic frameworks with anticipated porosities and functionalities. *CrystEngComm*, *16*(20), 4069–4083. https://doi.org/10.1039/C4CE00321G

25 Silva, P., Vilela, S. M. F., Tomé, J. P. C., & Almeida Paz, F. A. (2015). Multifunctional metal–organic frameworks: From academia to industrial applications. *Chemical Society Reviews*, *44*(19), 6774–6803. https://doi.org/10.1039/C5CS00307E

26 Zhinzhilo, V. A., Litvinova, A. Yu., Lyamina, V. M., Dzhardimalieva, G. I., & Uflyand, I. E. (2022). Coordinating Polymers Based on Nickel(II) and Cobalt(II) Trimesinates as Promising Adsorbents of Organic Dyes. *Bulletin of the University of Karaganda — Chemistry*, *107*(3), 239–253. https://doi.org/10.31489/2022Ch3/3-22-20

27 Dzhardimalieva, G., Zhinzhilo, V., & Uflyand, I. (2022). Advances in the chemistry of composites of metal-organic frameworks. *Russian Chemical Reviews*, *91*(10), 5055–5055. https://doi.org/10.57634/RCR5055

28 Si, J., Xia, H. -L., Zhou, K., Li, J., Xing, K., Miao, J., Zhang, J., Wang, H., Qu, L. -L., Liu, X. -Y., & Li, J. (2022). Reticular Chemistry with Art: A Case Study of Olympic Rings-Inspired Metal–Organic Frameworks. *Journal of the American Chemical Society*, *144*(48), 22170–22177. https://doi.org/10.1021/jacs.2c09832

29 Furukawa, H., Kim, J., Ockwig, N. W., O'Keeffe, M., & Yaghi, O. M. (2008). Control of Vertex Geometry, Structure Dimensionality, Functionality, and Pore Metrics in the Reticular Synthesis of Crystalline Metal−Organic Frameworks and Polyhedra. *Journal of the American Chemical Society*, *130*(35), 11650–11661. https://doi.org/10.1021/ja803783c

30 O'Keeffe, M. (2009). Design of MOFs and intellectual content in reticular chemistry: A personal view. *Chemical Society Reviews*, *38*(5), 1215. https://doi.org/10.1039/b802802h

31 Dybtsev, D. N., Yutkin, M. P., Peresypkina, E. V., Virovets, A. V., Serre, C., Férey, G., & Fedin, V. P. (2007). Isoreticular Homochiral Porous Metal−Organic Structures with Tunable Pore Sizes. *Inorganic Chemistry*, *46*(17), 6843–6845. https://doi.org/10.1021/ic7009226

32 Baimuratova, R. K., Andreeva, A. V., Uflyand, I. E., Shilov, G. V., Bukharbayeva, F. U., Zharmagambetova, A. K., & Dzhardimalieva, G. I. (2022). Synthesis and Catalytic Activity in the Hydrogenation Reaction of Palladium-Doped Metal-Organic Frameworks Based on Oxo-Centered Zirconium Complexes. *Journal of Composites Science*, *6*(10), 299. https://doi.org/10.3390/jcs6100299

33 Wang, D., Huang, R., Liu, W., Sun, D., & Li, Z. (2014). Fe-Based MOFs for Photocatalytic CO_2 Reduction: Role of Coordination Unsaturated Sites and Dual Excitation Pathways. *ACS Catalysis*, *4*(12), 4254–4260. https://doi.org/10.1021/cs501169t

34 Laurier, K. G. M., Vermoortele, F., Ameloot, R., De Vos, D. E., Hofkens, J., & Roeffaers, M. B. J. (2013). Iron(III)-Based Metal–Organic Frameworks As Visible Light Photocatalysts. *Journal of the American Chemical Society*, *135*(39), 14488–14491. https://doi.org/10.1021/ja405086e

35 Du, C., Zhang, Y., Zhang, Z., Zhou, L., Yu, G., Wen, X., Chi, T., Wang, G., Su, Y., Deng, F., Lv, Y., & Zhu, H. (2022). Fe-based metal organic frameworks (Fe-MOFs) for organic pollutants removal via photo-Fenton: A review. *Chemical Engineering Journal*, 431, 133932. https://doi.org/10.1016/j.cej.2021.133932

36 Zhang, H., Chen, S., Zhang, H., Fan, X., Gao, C., Yu, H., & Quan, X. (2019). Carbon nanotubes-incorporated MIL-88B-Fe as highly efficient Fenton-like catalyst for degradation of organic pollutants. *Frontiers of Environmental Science & Engineering*, *13*(2), 18. https://doi.org/10.1007/s11783-019-1101-z

37 Laurier, K. G. M., Vermoortele, F., Ameloot, R., De Vos, D. E., Hofkens, J., & Roeffaers, M. B. J. (2013). Iron(III)-Based Metal–Organic Frameworks As Visible Light Photocatalysts. *Journal of the American Chemical Society*, *135*(39), 14488–14491. https://doi.org/10.1021/ja405086e

38 Baati, T., Njim, L., Neffati, F., Kerkeni, A., Bouttemi, M., Gref, R., Najjar, M. F., Zakhama, A., Couvreur, P., Serre, C., & Horcajada, P. (2013). In depth analysis of the in vivo toxicity of nanoparticles of porous iron(III) metal–organic frameworks. *Chemical Science*, *4*(4), 1597. https://doi.org/10.1039/c3sc22116d

39 Serre, C., Mellot-Draznieks, C., Surblé, S., Audebrand, N., Filinchuk, Y., & Férey, G. (2007). Role of Solvent-Host Interactions That Lead to Very Large Swelling of Hybrid Frameworks. *Science*, 315(5820). https://doi.org/10.1126/science.1137975

40 Serre, C., Millange, F., Surblé, S., & Férey, G. (2004). A Route to the Synthesis of Trivalent Transition-Metal Porous Carboxylates with Trimeric Secondary Building Units. *Angewandte Chemie International Edition*, 43(46), 6285–6289. https://doi.org/10.1002/anie.200454250

41 Baimuratova, R. K., Zhinzhilo, V. A., Uflyand, I. E., Dmitriev, A. I., Zhidkov, M. V., Ovanesyan, N. S., Kugabaeva, G. D., & Dzhardimalieva, G. I. (2023). Low-Temperature Synthesis of Metal–Organic Coordination Polymers Based on Oxo-centered Iron Complexes: Magnetic and Adsorption Properties. *Russian Journal of Physical Chemistry A*, *97*(4), 735–748. https://doi.org/10.1134/S0036024423040064

42 He, J., Zhang, Y., Zhang, X., & Huang, Y. (2018). Highly efficient Fenton and enzyme-mimetic activities of NH2-MIL-88B(Fe) metal organic framework for methylene blue degradation. *Scientific Reports*, *8*(1), 5159. https://doi.org/10.1038/s41598-018-23557-2

43 Bondarenko, L., Baimuratova, R., Reindl, M., Zach, V., Dzeranov, A., Pankratov, D., Kydralieva, K., Dzhardimalieva, G., Kolb, D., Wagner, F. E., & Schwaminger, S. P. (2024). Dramatic change in the properties of magnetite-modified MOF particles depending on the synthesis approach. *Heliyon*, e27640. https://doi.org/10.1016/j.heliyon.2024.e27640

44 Bondarenko, L., Baimuratova, R., Dzeranov, A., Pankratov, D., Kicheeva, A., Sushko, E., Kudryasheva, N., Valeev, R., Tropskaya, N., Dzhardimalieva, G., & Kydralieva, K. (2024). Fenton reaction-driven pro-oxidant synergy of ascorbic acid and iron oxide nanoparticles in MIL-88B(Fe). *New Journal of Chemistry*, 10.1039.D4NJ00963K. https://doi.org/10.1039/D4NJ00963K

45 Zhang, C.-F., Qiu, L.-G., Ke, F., Zhu, Y.-J., Yuan, Y.-P., Xu, G.-S., & Jiang, X. (2013). A novel magnetic recyclable photocatalyst based on a core–shell metal–organic framework Fe3O4@MIL-100(Fe) for the decolorization of methylene blue dye. *Journal of Materials Chemistry A*, *1*(45), 14329. https://doi.org/10.1039/c3ta13030d

46 Yadav, S., Dixit, R., Sharma, S., Dutta, S., Solanki, K., & Sharma, R. K. (2021). Magnetic metal–organic framework composites: Structurally advanced catalytic materials for organic transformations. *Materials Advances*, *2*(7), 2153–2187. https://doi.org/10.1039/D0MA00982B

47 Rahim Pouran, S., Abdul Raman, A. A., & Wan Daud, W. M. A. (2014). Review on the application of modified iron oxides as heterogeneous catalysts in Fenton reactions. *Journal of Cleaner Production*, *64*, 24–35. https://doi.org/10.1016/j.jclepro.2013.09.013

48 Dzhardimalieva, G. I., Irzhak, V. I., Bratskaya, S. Yu., Maiorov, V. Yu., Privar, Yu. O., Kasymova, E. D., Kulyabko, L. S., Zhorobekova, Sh. Zh., & Kydralieva, K. A. (2020). Stabilization of Magnetite Nanoparticles in Humic Acid Medium and Study of Their Sorption Properties. *Colloid Journal*, *82*(1), 1–7. https://doi.org/10.1134/S1061933X20010032

49 Sapianik, A. A., Kiskin, M. A., Kovalenko, K. A., Samsonenko, D. G., Dybtsev, D. N., Audebrand, N., Sun, Y., & Fedin, V. P. (2019). Rational synthesis and dimensionality tuning of MOFs from preorganized heterometallic molecular complexes. *Dalton Transactions*, *48*(11), 3676–3686. https://doi.org/10.1039/C8DT05136D

50 Elmore, W. C. (1938). Ferromagnetic Colloid for Studying Magnetic Structures. *Physical Review*, *54*(4), 309–310. https://doi.org/10.1103/PhysRev.54.309

51 Savitzky, A., & Golay, M. J. E. (1964). Smoothing and Differentiation of Data by Simplified Least Squares Procedures. *Analytical Chemistry*, *36*(8), 1627–1639. https://doi.org/10.1021/ac60214a047

52 Dzeranov, A., Pankratov, D., Bondarenko, L., Telegina, L., Dzhardimalieva, G., Saman, D., & Kydralieva, K. (2024). Humic acids-modified mesoporous silica encapsulating magnetite: Crystal and surface characteristics. *CrystEngComm*. https://doi.org/10.1039/D4CE00281D

53 Ma, B., Wang, S., Liu, F., Zhang, S., Duan, J., Li, Z., Kong, Y., Sang, Y., Liu, H., Bu, W., Li, L. (2018). Self-assembled copper-amino acid nanoparticles for in situ glutathione "and" H_2O_2 sequentially triggered chemodynamic therapy. *Journal of the American Chemical Society*, *141*, 849–857. https://doi.org/10.1021/jacs.8b08714

54 Hernandez, J. S. T., Aragón-Muriel, A., Corrales Quintero, W., Castro Velásquez, J. C., Salazar-Camacho, N. A., Pérez Alcázar, G. A., & Tabares, J. A. (2022). Characterization of Fe_3O_4 Nanoparticles for Applications in Catalytic Activity in the Adsorption/Degradation of Methylene Blue and Esterification. *Molecules*, *27*(24). https://doi.org/10.3390/molecules27248976

55 Wang, B., Yin, J.-J., Zhou, X., Kurash, I., Chai, Z., Zhao, Y., & Feng, W. (2013). Physicochemical Origin for Free Radical Generation of Iron Oxide Nanoparticles in Biomicroenvironment: Catalytic Activities Mediated by Surface Chemical States. *The Journal of Physical Chemistry C*, *117*(1), 383–392. https://doi.org/10.1021/jp3101392

56 Voinov, M. A., Pagán, J. O. S., Morrison, E., Smirnova, T. I., & Smirnov, A. I. (2011). Surface-Mediated Production of Hydroxyl Radicals as a Mechanism of Iron Oxide Nanoparticle Biotoxicity. *Journal of the American Chemical Society, 133*(1), 35–41. https://doi.org/10.1021/ja104683w

57 Hermanek, M., Zboril, R., Medrik, I., Pechousek, J., & Gregor, C. (2007). Catalytic Efficiency of Iron(III) Oxides in Decomposition of Hydrogen Peroxide: Competition between the Surface Area and Crystallinity of Nanoparticles. *Journal of the American Chemical Society, 129*(35), 10929–10936. https://doi.org/10.1021/ja072918x

58 Wang, F., Pauletti, G. M., Wang, J., Zhang, J., Ewing, R. C., Wang, Y., & Shi D. (2013). Dual surface functionalized janus nanocomposites of polystyrene/Fe_3O_4@SiO_2 for simultaneous tumor cell targeting and stimulus-induced drug release. *Advanced Materials, 25*, 3485–3489. https://doi.org/10.1002/adma.201301376